Impact of Multialtimeter Sea Level Assimilation in the Mediterranean Forecasting Model

M.-I. PUJOL

Gruppo di Oceanografia Operativa, Istituto Nazionale di Geofisica e Vulcanologia, Bologna, Italy

S. DOBRICIC

Centro Euro-Mediterraneo per i Cambiamenti Climatici, Bologna, Italy

N. PINARDI

Centro Interdipartimentale per la Ricerca sulle Scienze Ambientali, Alma Mater Studiorum Università di Bologna, Ravenna, Italy

M. ADANI

Centro Euro-Mediterraneo per i Cambiamenti Climatici, Bologna, Italy

(Manuscript received 17 June 2009, in final form 16 June 2010)

ABSTRACT

In this article the impact of multisatellite altimeter observations assimilation in a high-resolution Mediterranean model are analyzed. Four different altimeter missions [*Jason-1*, *Envisat*, Ocean Topography Experiment (TOPEX)/Poseidon interleaved and *Geosat Follow-On*] are used over a 7-month period (from September 2004 to March 2005) to study the impact of the assimilation of one to four satellites on the analyses quality. The study highlights three important results. First, it shows the positive impact of the altimeter data on the analyses. The corrected fields capture missing structures of the circulation, and eddies are modified in shape, position, and intensity with respect to the model simulation. Second, the study demonstrates the improvement in the analyses induced by each satellite. The impact of the addition of a second satellite is almost equivalent to the improvement given by the introduction of the first satellite: the second satellite's data bring a 12% reduction of the root-mean-square of the differences between the analyses and observations for the sea level anomaly (SLA). The third and fourth satellites also improve the rms, with a more than 3% reduction for each of them. Finally, it is shown that *Envisat* and *Geosat Follow-On* additions to *Jason-1* impact the analyses more than the addition of TOPEX/Poseidon, suggesting that the across-track spatial resolution is still one of the important aspects of a multimission satellite observing system. This result could support the concept of multimission altimetric monitoring done by complementary horizontal resolution satellite orbits.

1. Introduction

During the recent decades numerical model simulations have considerably contributed to a new understanding of the ocean circulation and its variability. Model simulations have become more realistic and allow the exploration of the synoptic scales of the ocean circulation in a way that could never be achieved with sparse in situ measurements. The realism of the model outputs can be strongly improved by data assimilation of in situ and satellite data. In particular, the altimeter data provide key observations that are used to correct the model because they have almost uniform and regular coverage with a high revisit time period (De Mey and Robinson 1987; Fukumori et al. 1999; Dobricic et al. 2005).

Since the beginning of altimetry, the question of the optimal spatial and temporal coverage of satellites in view of assimilation into numerical models has been studied. Mellor and Ezer (1991) showed that low-altimeter spatial sampling could increase the rms error by about 2–3 times with respect to a finer sampling. Moreover, they showed

Corresponding author address: M.-I. Pujol, CLS-DOS, 8-10 rue Hermes, Parc Technologique du canal, 31520 Ramonville Saint-Agne, France.
E-mail: mpujol@cls.fr

that error associated with imperfect altimeter coverage is larger than the error associated with imperfect parameterization of surface to subsurface correlation involved in assimilation technique. However, in a single satellite assimilation context, spatial and temporal sampling could not be dissociated. Berry and Marshall (1989) showed that an altimeter with a 14-day repeat period (with a 140-km track separation in the studied area) gave optimal results. However, as shown by Holland and Malanotte-Rizzoli (1989), when assimilating along altimeter tracks, the trade-off between space and time resolution just about compensate for each other. As underlined by the same authors, the results depends on the assimilation technique and parameterizations and also on space and time scales of motion in the region studied and capacity of the model to reproduce these structures and variability.

Since 1992 multialtimetry data have been available (Le Traon 2002) and numerical models have increased the spatial resolution, reaching a few kilometers horizontal grid spacing, and the question of the optimal altimeter sampling scheme in a model assimilation context can be reviewed. Recent studies (Benkiran 2007) focused on the question of the optimal spatial and temporal coverage of the satellite in view of the assimilation in numerical models. Benkiran (2007) made the first estimation of the impact of the assimilation of four satellites into an oceanographic data analysis system of the northern Atlantic, and he found that the impact of the addition of a fourth satellite was insignificant. However, his result was obtained by a coarse spatial resolution model setup ($\frac{1}{3}°$) and the weekly assimilation window.

In this study we will estimate the impact of the multimission spatial/temporal coverage on the analyses of the Mediterranean Forecasting System (MFS; Pinardi et al. 2003; N. Pinardi and Coppini 2010, unpublished manuscript). The numerical model has a resolution of $\frac{1}{16}°$ latitude $\times$ $\frac{1}{16}°$ longitude (approximately 6.5 km), and it is able to represent eddies because the first Rossby radius of deformation is 10 km. Eddies in the Mediterranean are pervasive (Millot 1999; Millot and Taupier-Letage 2005; Robinson et al. 2001), and the reproduction of mesoscales in the sea surface variability is a key parameter that is used to judge the quality of the assimilation and model system. Furthermore, we will assess the optimal satellite multimission monitoring parameters by estimating how each of the four satellites, characterized by different sampling schemes, impacts the analysis quality.

The study is focused on the period from September 2004 to March 2005 during which four different altimeters were active. Different assimilation experiments for the various altimeter combinations are shown. They are described in section 2 after a brief presentation of the MFS model and the assimilation method used. The high-resolution error covariance matrix used for this study is presented in section 3. Analysis fields are compared with sea level anomaly (SLA) and Argo independent data to estimate the quality of the analyses. The results obtained are discussed in section 4 in terms of improvement of the root-mean-square error for SLA, temperature, and salinity. Section 5 summarizes and offers the conclusions.

2. Data and methods

a. The MFS model and its assimilation scheme

The MFS model is based on the Océan Parallélisé (OPA) 8.2 code (Madec et al. 1998) with an implicit free surface. One of the interesting characteristics of this model is its high horizontal and vertical resolution: it reaches a $\frac{1}{16}° \times \frac{1}{16}°$ horizontal resolution (i.e., approximately 6.5 km) and 72 vertical levels unevenly spaced in order to increase the resolution near the surface. A detailed description of the model is given in Tonani et al. (2008).

To assimilate observations, the MFS model is combined with a three-dimensional variational data assimilation (3DVAR) ocean scheme (OceanVar; Dobricic and Pinardi 2008; also see the appendix herein). For this study, both SST and altimeter data were assimilated. The SST assimilation is done by correcting the surface heat fluxes, as explained in Pinardi et al. (2003), with a term that is proportional to the difference between the model temperature at the surface and the observational SST. The latter is produced daily by an objective analysis scheme developed by Buongiorno Nardelli et al. (2003).

In the OceanVar scheme, the background error covariance is subdivided into a sequence of operators (Dobricic and Pinardi 2008), with one of them containing statistically estimated vertical error covariances of temperature and salinity, which is a key element for the assimilation of SLA observations as explained in Dobricic et al. (2007). They are represented by multivariate empirical orthogonal functions (EOFs) computed from a 9-yr model simulation (from 1993 to 2001). New EOFs were computed specifically for this study. The method and the resulting EOFs are presented in the section 3.

Assimilation can be used for various purposes (Robinson and Lermusiaux 2001; Lermusiaux et al. 2006). In this paper the data assimilation system is used to correct the model background (or first guess) fields by combining them with the information from the observations. To do so it is necessary to make sure that the observed and background quantities are comparable. The altimeter measurements are given as SLA obtained by subtracting a long-term mean of the satellite data, the so-called mean

sea surface height (MSSH), for the period of 1993–99. To compute the model SLA, a mean dynamic topography (MDT) is removed from the model sea surface height. This MDT is estimated from model output and data for the same period that characterizes the MSSH (Rio et al. 2007), and is further corrected by long-term assimilation diagnostics (Dobricic 2005).

The altimeter SLA signal gives the time-dependent dynamical part of the sea level variations (frequencies higher than 0.05 days^{-1} have been removed). They correspond to barotropic aliased signals (Carrère and Lyard 2003), which contain a multiplicity of time scales. A major part of the SLA signal is induced by long time-scale signals, such as the steric effect (seasonal variability of water masses); another part is due to mean current variability (seasonal-to-interannual variability) and shorter time variability, which is mainly dominated by mesoscale structures (<200 km).

In the model, the sea surface is a prognostic variable. It represents the dynamic height induced by large-scale forcing of the circulation (wind, water, and heat fluxes) and by the mesoscales. Because the model is incompressible and Boussinesq, which, at zeroth order, implies incompressible flows, the steric contribution to sea level averaged over the whole model domain does not contribute to the dynamics (Mellor and Ezer 1995) and should be excluded from the model–data misfit, as explained in Demirov et al. (2003). Because our model domain is closed we must remove the steric effect from the observations. We remove it by subtracting the mean of the misfits along each satellite track. The amplitude of the steric oscillation in the Mediterranean is similar to that in the North Atlantic, where it is about 10–20 cm (Ivchenko et al. 2007; Oddo et al. 2009). The ocean thermal expansion is slow, and therefore it can be easily estimated by calculating the basin-averaged SLA once a week. However, there are other large-scale effects that are not simulated by the model and have shorter time scales. For example, the inverse barometer is removed from SLA observations by using the ECMWF atmospheric pressure analyses that contain some uncertainty. Furthermore, because the only connection to the global ocean is through the narrow Strait of Gibraltar, rapidly moving atmospheric pressure disturbances produce barotropic oscillations that may affect the sea level in the Mediterranean for several days (Le Traon and Gauzelin 1997). The local variability of the wind in the Strait of Gibraltar, which is poorly represented in the European Centre for Medium-Range Weather Forecasts (ECMWF) wind analyses, may produce high-frequency oscillations of the mean sea level in the Mediterranean (Fukumori et al. 2006). The intercalibration (Le Traon and Ogor 1998) process removes most of the high-frequency barotropic

oscillations from the observations, but it could leave some biased high-frequency oscillations at smaller spatial scales. In the MFS operational system it was found that by removing the mean misfit along each track (Dobricic et al. 2005) the rms error for SLA was reduced by about 10%–20% with respect to the subtraction of the climatological estimate of the steric height (Demirov et al. 2003).

In this paper we follow this nomenclature: $\mathbf{X}^a = [T, S, \eta]^{\mathrm{T}}$ is the analysis state vector containing all of the gridpoint values of temperature, salinity, and sea level; $\mathbf{X}^b = [T, S, \eta]^{\mathrm{T}}$ is the background or first-guess model field that we want to improve with assimilation; and $\mathbf{Y}^O$ is the observational quantity. The assimilation scheme computes misfits, or the differences between the observations and the model first guess before the analysis. The analyses correct not only the sea level but also other model-state variables, in particular, temperature and salinity vertical profiles through the vertical and horizontal components of the background error covariances (Dobricic and Pinardi 2008).

The assimilation cycle is daily and the correction of the model fields is done in filter mode (Demirov et al. 2003); that is, only observations in the past are used to produce an analysis. Every day, up to 600 SLA data points for that day are assimilated along different tracks in the Mediterranean Sea. It should be mentioned that Archiving, Validation, and Interpretation of Satellite Oceanographic data (AVISO; AVISO 2009) provides composed gridded datasets that can be successfully assimilated into ocean models (e.g., Oey et al. 2005). The AVISO gridded product is daily (near-real-time product); however, short frequencies are "averaged" in the gridding process (AVISO uses a 3-week temporal window). The key difference between the two approaches (using along-track data and objectively analyzed sea surface height maps) is the fact that by using directly along-track altimeter data we allow for the high-frequency signal to be assimilated. Although our approach requires more careful preprocessing of the along-track data, it is more general and does not preclude the inclusion of all space and time frequencies of the observations in the assimilation scheme.

The resulting analyses for sea level η, temperature T, and salinity S are compared after assimilation to the observations in order to estimate a difference vector $\mathbf{D}$, defined as

$$\mathbf{D} = \mathbf{Y}^O - H(\mathbf{X}^a), \qquad (1)$$

where H is a simple bilinear interpolation to the observational spatial and temporal point and $\mathbf{X}^a$ is the analysis state vector. These differences are an estimate of the agreement of the analysis with observations. The mean

TABLE 1. Between track distances (in the Mediterranean Sea) and repeat view characteristics of each altimeter used.

	$J1$ and T/P	$G2$	EN
Between track distance in the Mediterranean Sea (km)	~260	~130	~65
Repeat view (days)	10	17	35

of the vector values of $|\mathbf{D}|$ and the square root of the mean of $|\mathbf{D}|^2$ will be called the bias and root-mean-square (rms) of the posterior residuals [or "analyses minus observations" (AMO)], respectively. For SLA differences, the mean is subtracted along each track, as done for the misfits, in order to eliminate the steric effect. For SLA in particular, we calculated the mean of the absolute value of AMO.

b. The altimeter data

The altimeter data used in this study are along-track, near-real-time data distributed by AVISO. Data from the following four altimeters were collected: *Jason-1* (*J1*), Ocean Topography Experiment (TOPEX)/Poseidon (T/P), *Envisat* (*EN*), and *Geosat Follow-On* (*G2*); they were geophysically corrected (tides, wet and dry tropospheric, and ionospheric corrections). The low-frequency inverse barometer effect and high-frequency barotropic response to wind and pressure forcing given by the Modèle aux Ondes de Gravité 2 Dimensions (MOG2D; Carrère and Lyard 2003) was removed to the altimeter signal. This allowed for an improved correction of aliasing effect induced by the satellite's repetition of the measurement. All of the data were intercalibrated, performing a global crossover adjustment using *J1* as the reference mission (Le Traon and Ogor 1998). Along-track data were resampled every 7 km using cubic splines. SLAs were computed by removing a 7-yr mean sea surface height

corresponding to the period of 1993–99. Finally, measurement noise was reduced by applying Lanczos (having a cutoff wavelength of 42 km) and median (21 km) filters. The data were then subsampled every ~14 km in order to limit the number of redundant observations.

The characteristics of the different altimeter sampling schemes are given in Table 1. The *J1* mission and T/P present the best temporal revisit time but have low spatial resolution. Note that T/P tracks are located between the *J1* during the tandem mission (September 2002–October 2005). The combination of *J1* and T/P thus allows optimal spatial coverage. However, the combination with temporal coverage is limited because the two satellites are flying side by side. Contrary to *J1*, *EN* presents a higher spatial coverage but a longer revisit period; *G2* characteristics are halfway between *J1* and *EN*.

c. Independent data for validation

Argo data are now a consistent real-time input data for assimilation and validation in the Mediterranean Sea (Poulain et al. 2007). Nearly 700 vertical profiles were collected during the studied period. The position of the different Argo profiles used is shown in Fig. 1. In this study, Argo data are used the first time as an assimilated dataset in order to verify the robustness of the background error covariance matrix (section 3). In a second instance, Argo profiles are used as a completely independent dataset (section 4). All of the statistics computed for AMO by Eq. (1) with $\mathbf{X}^a$ at day J consider observations at day $J + 1$. In this way, even when temperature and salinity observed by Argo floats are assimilated (this is done only for the validation of the background error covariance matrix in section 3), it can be assumed that AMO represent an independent dataset for the validation. In the Mediterranean the Argo profiles occur every 5 days, and with a correlation scale
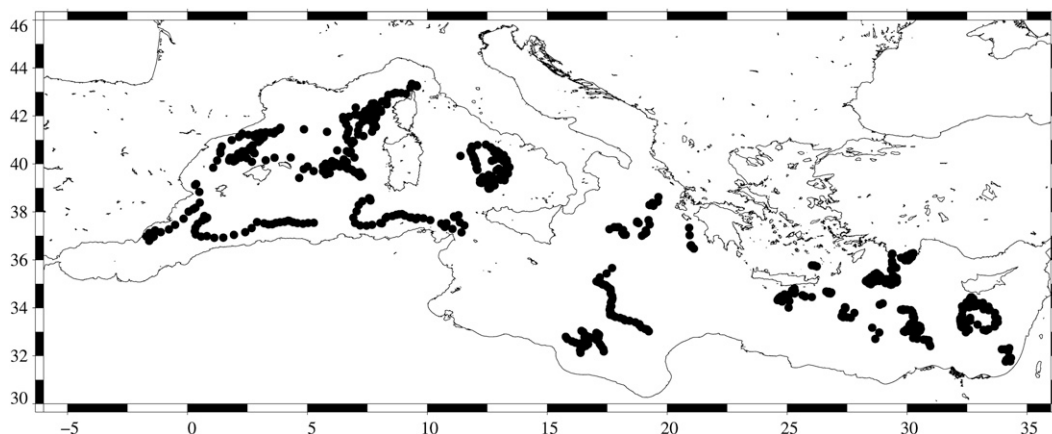

FIG. 1. Position of the different Argo profiles for the period of September 2004–March 2005.

TABLE 2. Summary of the experiments as a function of the number of altimeters.

Experiment	Exp0	Exp1	Exp2a	Exp2b	Exp3	Exp4	Exp4TS
Altimeter used	—	$J1$	$J1 + EN$	$J1 + $ T/P	$J1 + EN$ $+$ T/P	$J1 + EN + $ T/P $+ G2$	$J1 + EN + $ T/P $+ G2$ $+ $ Argo (T/S) + XBT(T)

of 10 km the drifter only needs an average motion of 2 cm s^{-1} to be in an independent location. Furthermore, Argo observations on day J and day $J + 1$ are made by different floats. Therefore, it may be reasonable to assume that the differences between model fields in two consecutive days will be smaller than the differences between those fields and the verifying observations.

SST and color data are used for a qualitative validation of the posterior ocean estimates. These data are used as gridded maps, which are 10-day averages built from Moderate Resolution Imaging Spectroradiometer (MODIS) level 2 products downloaded from the Ocean Color Web (http://oceancolor.gsfc.nasa.gov). They are compared with the SSH model output.

d. The numerical experiments

Five experiments are illustrated in this paper. They are done in order to analyze the impact of the different background error covariance matrix and to test various satellite combinations and their impact on the analysis quality. Each experiment covers the period from September 2004 to March 2005. The only difference between the experiments is the number of altimeter data assimilated and the optional assimilation of Argo and XBT profiles.

The different combinations of satellites used in the experiments are summarized in Table 2. The reference experiment does not assimilate altimeter data (Exp0). In experiment 1 (Exp1), only $J1$ data are assimilated. Then, two dual-satellite combinations are tested in experiments 2a and 2b (Exp2a and Exp2b); in the first one (Exp2a), we consider the combination $J1 + EN$, combining thereby the respective high temporal and spatial sampling characteristics of each satellite. In Exp2b, the duo $J1 + $ T/P interleaved is used, supposedly offering optimal coverage (Chelton and Schlax 2003). In experiment 3 (Exp3), data from $J1$, EN, and T/P are combined. Finally, in experiment 4 (Exp4), data from the four satellites ($J1$, EN, T/P, and $G2$) are assimilated.

An additional experiment (Exp4TS), assimilating four altimeters as well as Argo (T/S) and XBT profiles, is carried out to analyze the impact of different background error covariance matrices.

An SST relaxation was applied to all of the experiments.

3. Computation of the background vertical error covariance matrix

Data assimilation requires the knowledge of the spatial/temporal structure of the background error covariances. In OceanVar (see the appendix), the background error covariances of temperature and salinity are estimated successively in vertical and horizontal directions. SLA error covariances are then estimated as the steady-state solution of a barotropic oceanographic model simulation forced by temperature and salinity error covariances. The accuracy of the analyses of T and S thus strongly depends on the quality of the estimated covariances of temperature and salinity in the vertical direction. In Dobricic and Pinardi (2008), vertical error covariances between temperature and salinity are statistically estimated with vertical EOF defined for 13 regions of the Mediterranean Sea and seasonal temporal resolution. Throughout, we will refer to them as low-resolution EOF (LR EOF) because they have low spatial and temporal resolution. Here we describe the methodology used to compute higher-resolution EOFs that should better fit the model resolution and its capability to represent smaller spatial scales. We will also show the importance of this part of the error covariance matrix for the quality of temperature and salinity corrections.

The multivariate vertical error covariance EOFs are estimated considering the covariance matrix between temperature, salinity, and sea level, as described in Dobricic et al. (2005). The matrix scaling is described in detail in Dobricic et al. (2005), and here we will say only that we considered a depth-constant variance and the geometrical scaling. This was shown to be necessary in order to maintain the largest scaled errors in the thermocline. A 9-yr (1993–2001) simulation is used to define the vertical error covariance matrix and to compute new multivariate vertical EOFs (HR EOFs; these EOFs have a higher spatial and temporal resolution with respect to LR EOF). The model domain is subdivided into $1/4° \times 1/4°$ boxes and for each of them vertical monthly EOFs are computed. Each box overlaps by an area of $3/4° \times 3/4°$ and considers 6 weeks of data around the central time of each month. This was done to ensure a smooth transition from an area/month to the other. Inside each box, only grid points deeper than 500 m were selected so that EOFs were calculated, and assimilation was carried out,
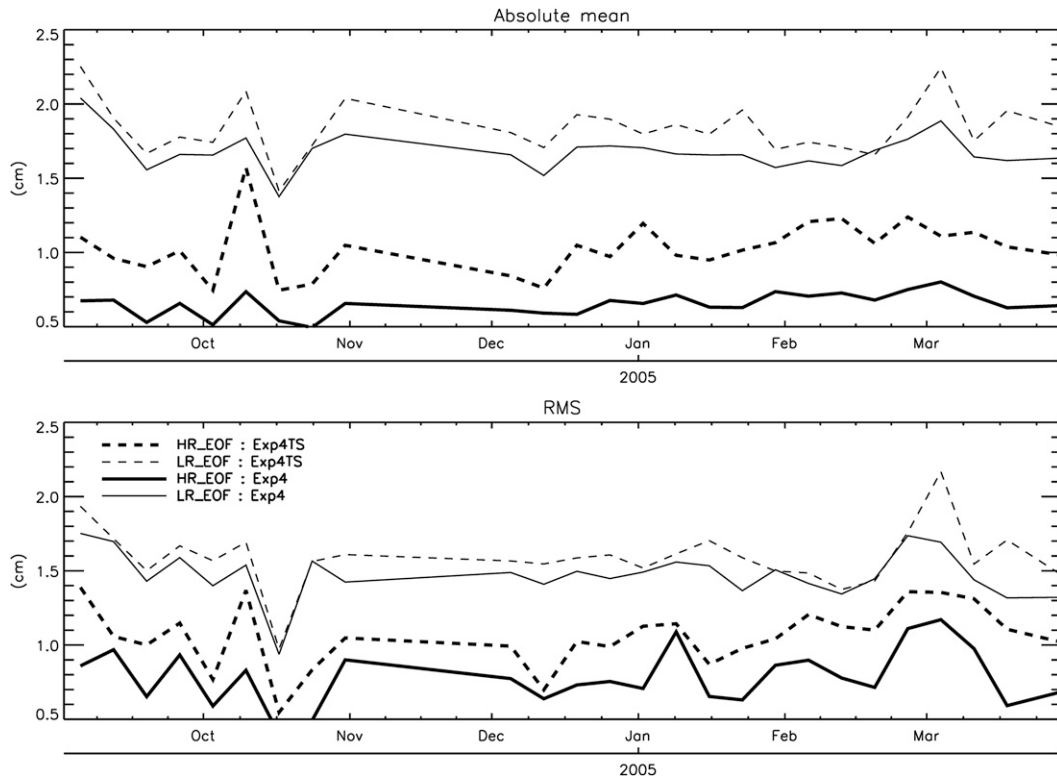
FIG. 2. Temporal evolution of the 7-day (top) absolute value and (bottom) rms of AMO for SLA. SLA data assimilated with LR EOFs (continuous thin line); SLA data assimilated with HR EOFs (continuous thick line); SLA, ARGO, and XBT data assimilated with LR EOFs (dashed thin line); and SLA, Argo, and XBT data assimilated with HR EOFs (dashed thick line).

for depths greater than 500 m. The maximum number of data available at each grid depth was used to define the maximum depth (Zmax) for each area and EOF.

Performances of these new vertical EOFs are estimated in terms of analysis error reduction over the period of September 2004–March 2005. To detect the improvements resulting from the higher spatial resolution of EOFs, Exp4 and Exp4TS using HR EOFs and LR EOFs are compared with available observations. The mean absolute value of the bias and rms of AMO for SSH and temperature and salinity profiles are used to estimate the quality of the analyses.

Figure 2 presents the temporal evolution of the 7-day mean of the absolute value of the bias and the rms of AMO when either HR EOFs or LR EOFs are used. The results clearly show a net reduction of the mean absolute value when HR EOFs are used with respect to the results obtained with LR EOFs. The reduction of the mean absolute value of the bias and its variance is given in Table 3 in terms of the percentage of the signal with an associated error (bootstrap method). HR EOFs allows a reduction of 61% ($\pm$3%) of the mean absolute value of the bias and 45% ($\pm$6%) of the rms with respect

to the LR EOFs when only SLA data are assimilated. The introduction of Argo and XBT data leads to a lower reduction of the SLA bias and rms ($\sim$45% and $\sim$33%, respectively, see Table 3). This is probably due to the fact that temperature and salinity corrections inferred from SLA misfits are not entirely consistent with their corrections calculated from misfits of Argo and XBT. However, it should be noticed that the mean absolute value of the bias and the rms of AMO do not represent a reliable measure for the quality of the analyses, because SLA observations are assimilated. They only show the level of the agreement between the analyses and the

TABLE 3. Reduction of the absolute bias and rms of AMO for SLA, induced by the use of HR EOFs with respect to the use of LR EOFs. Values are given in percent of the signal with an associated error corresponding to the 95% confidence interval.

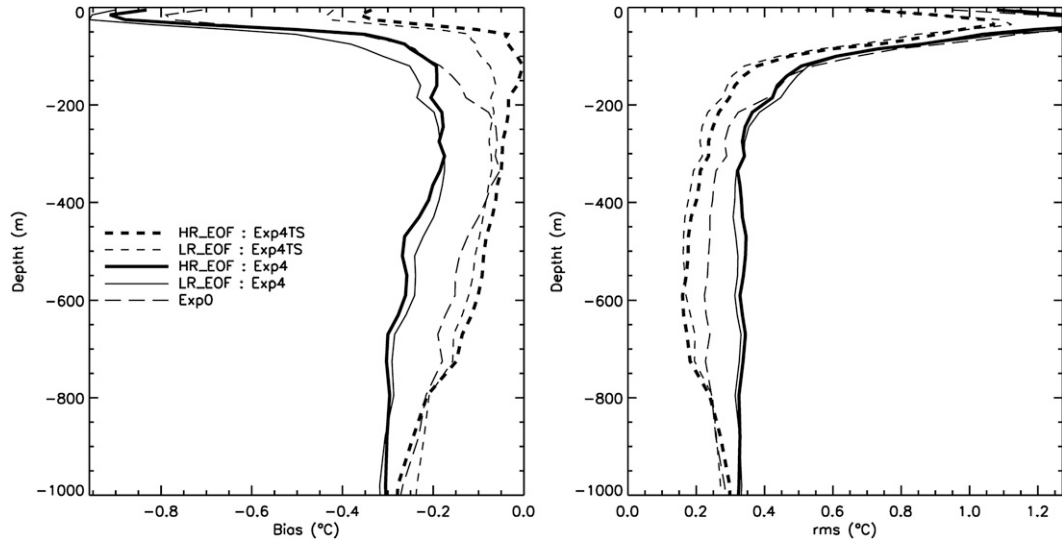|	Reduction of the absolute bias	Reduction of the rms
Four satellites assimilated	-61 ± 3	-45 ± 6
Four satellites + Argo + XBT data assimilated	-45 ± 4	-33 ± 5

FIG. 3. Vertical distribution of the (left) bias and (right) rms of AMO for temperature profiles.

observations. For example, a higher agreement represented by a lower rms of AMO may simply reflect higher background error variances for the sea level. All of the experiments give the mean absolute value of the bias and the rms of AMO, which is within the estimated error of observations of 2–3 cm (Ducet et al. 2000; Ménard et al. 2003). Therefore, the two sets of EOFs give equally probable analyses of the SLA either with or without the addition of XBT and Argo profiles.

Performances of HR EOFs were also analyzed by the evaluation of the bias and rms of AMO for temperature and salinity profiles using Argo observations. AMO are calculated a posteriori, as discussed in section 2c, by spatially interpolating the temperature and salinity analyses on day J to observational points on day $J + 1$ and by subtracting the observed values on day $J + 1$. Results are presented in Figs. 3 and 4 for temperature and salinity profiles, respectively. The reduction of the bias and the rms of AMO (in terms of the percent of the Exp0 signal) in the upper 400 m are reported in Table 4.

Assimilation of the SLA observations (Exp4) tends to increase the bias of temperature AMO with respect to the model without the assimilation (Exp0; see Fig. 3a and Table 4). Spatial resolution of the background vertical error covariances has a low impact, but an overall lower bias is obtained when HR EOFs are used,
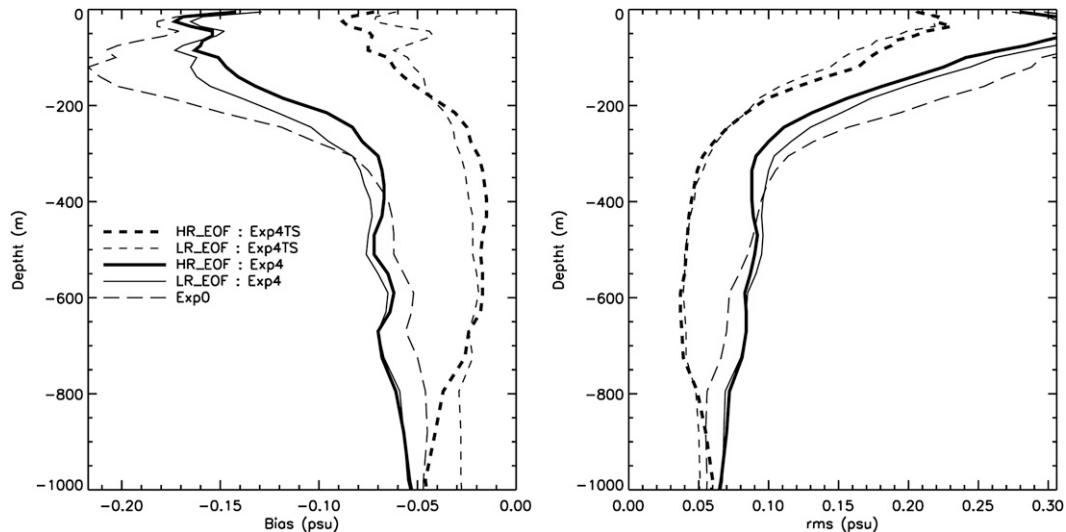

FIG. 4. Vertical distribution of the (left) bias and (right) rms of AMO for salinity profiles.

TABLE 4. Reduction (%) of AMO bias and rms in the upper 400 m, for temperature and salinity.

	LR EOFs		HR EOFs						
	Exp0 → Exp4	Exp0 → Exp4TS	Exp0 → Exp4	Exp0 → Exp4TS	Exp0 → Exp1	Exp1 → Exp2a	Exp1 → Exp2b	Exp2a → Exp3	Exp3 → Exp4
Bias T	+61	−41	+43	−65.5	+20	+11	−7	−1	−9
Bias S	−14	−72	−22	−70	−11	−4	−4	−3	−7
Rms T	+8	−27.5	+4.5	−23	+15	−13	−7	+3	1
Rms S	−13	−49	−19	−47	−7	−8	−5	0	−6

especially in the upper 300 m. The bias of AMO for temperature is approximately 20% smaller when HR EOFs are used instead of LR EOFs. The rms of AMO for Exp4 with both HR EOF and LR EOF is impacted by the observed bias (Fig. 3b and Table 4). Rms is actually about 8%–4.5% higher than that for Exp0. However, the analysis of variability of AMO shows a reduction of about 2%–3% (respectively, for LF EOFs and HR EOFs). Overall, the different EOFs have a small impact on the quality of the analyses in term of AMO variability, and they produce a larger bias when only SLA data are assimilated.

When Argo and XBT profiles are assimilated in addition to SLA data (Exp4TS), the bias and rms of AMO temperature is largely reduced for both LR EOF and HR EOF, and HR EOF leads to a nearly 20% higher reduction of the bias than when LR EOF are used (Fig. 3a and Table 4). In the same way, the rms of the AMO temperature is significantly reduced, reaching 23% and 27.5% of the Exp0 signal for HR EOF and LR EOF (Fig. 3b and Table 4).

Considering the salinity now, Exp4 improves with respect to Exp0 (Fig. 4). A significant reduction of the bias and the rms of AMO salinity is observed especially in the upper 300 m. Best results are obtained when HR EOF are used. In this case, salinity bias reduction in Exp4 reaches up to 22% of the signal and rms is reduced up to 19% with respect to Exp0 (Table 4). When Argo and XBT data are also assimilated, the results are again largely improved, with slightly higher performances for LF EOFs. In this case, AMO salinity bias reduction reaches 70% and 72% of the Exp0 signal for HR EOFs and LR EOFs, respectively. The AMO rms reduction is 47% and 49% for HR EOFs and LR EOFs, going from Exp0 to Exp4TS.

The obtained results underline the limits and the accuracy of the data assimilation scheme used in this study. As mentioned before, Figs. 3 and 4 show that the temperature bias and rms error in Exp4 is larger than that in Exp0, and the result is not sensitive to the different EOF sets used. The degradation of the bias and rms is small however, on the order of 0.2°C, and this sets the accuracy of our method for correcting temperature. In the past,

assimilation of satellite altimeter data (Ezer and Mellor 1994; Masina et al. 2001; Haines 2002) has been carried out with simpler methods and improvement between assimilation and no-assimilation experiments has been noticeably positive even if ARGO data were not available for a quantitative comparison. However, the models used in the past studies were much less skilled in reproducing the ocean variability and an estimate of the accuracy limit of the assimilation scheme was not possible. In our case, it seems that such a limit can be set at few tenths of a degree for temperature. For salinity the Exp0 error is much larger from the start and the assimilation overall improves.

In summary, section 3 shows that the assimilation skill is improved by using HR EOFs with respect to LR EOFs. Even if the benefit is more evident in the case of assimilation of both SLA and temperature and salinity profiles, we will use the HR EOF in all of the remaining experiments.

4. Impact of number of altimeters on analysis quality

a. Impact of number of altimeters on SLA analyses

The impact of the different satellite combinations on the quality of the analyzed SLA is estimated by computing AMO using (1), as done previously for temperature and salinity analysis. Considering results presented in section 3, experiments were performed by using HR EOFs. AMO is calculated for SLA observations by all four satellites. Those differences are calculated a posteriori, by spatially interpolating the SLA analyses on day J to observational points on day $J + 1$ and by subtracting the observed values on day $J + 1$. This may be done by assuming that mesoscale fields are highly correlated from one day to the other. Independent data validation will be done only for temperature and salinity profiles.

The temporal evolution of AMO rms for SLA is presented in Fig. 5. The difference was computed globally along all of the satellites tracks and for each altimeter independently in order to underline the impact of each altimeter. It is clear that the rms of AMO for SLA is
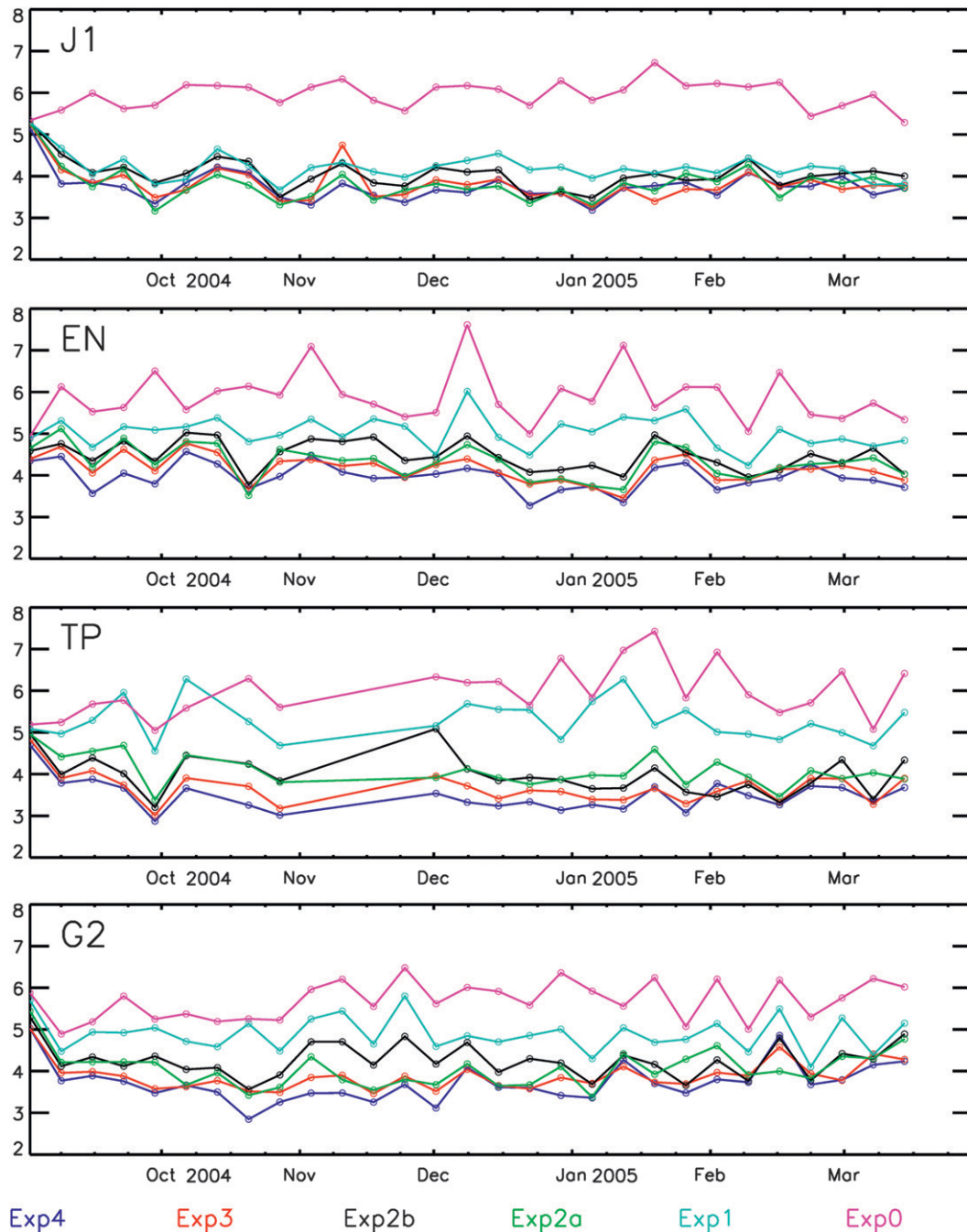
FIG. 5. Temporal evolution of the rms of AMO (cm) using along-track satellite data. (top to bottom) Differences along *J1*, *EN*, T/P, and *G2* tracks for the different experiments of Table 2.

reduced by assimilating all of the satellites. The assimilation of the four satellites (Exp4) gave the best results with a mean rms of AMO of ~4 cm, which is almost the rms error of the altimeter measurement (Ducet et al. 2000; Ménard et al. 2003); whereas when using *J1* data only (Exp1), the rms is almost 5 cm. Without assimilation of SLA (Exp0), the rms is almost 6 cm.

The reduction of the rms of AMO for SLA, expressed in percent of the signal between an experiment and the other and its 95% confidence interval, are given in Table 5. The rms steadily decreases with the addition of satellites. It is interesting to note in Table 5 that the impact of *EN* is slightly higher than the impact of T/P when added to *J1*. Considering *EN* as the second satellite with

TABLE 5. Reduction of the rms of the along-track SLA AMO: the difference is calculated along the different satellite tracks as a function of the different experiments. Values are given in percent of the signal with an associated error corresponding to the 95% confidence interval.

	Exp0 → Exp1	Exp1 → Exp2a	Exp1 → Exp2b	Exp2a → Exp3	Exp3 → Exp4
J1	−29 ± 3	−9 ± 4	−4 ± 4	+0 ± 5	−1 ± 5
EN	−15 ± 4	−14 ± 4	−11 ± 3	−4 ± 4	−5 ± 2
T/P	−12 ± 5	−23 ± 4	−25 ± 4	−10 ± 5	−5 ± 5
G2	−14 ± 3	−17 ± 4	−13 ± 4	−4 ± 5	−5 ± 5
All	−20 ± 2	−15 ± 3	−12 ± 3	−3 ± 4	−4 ± 4

J1 (Exp2a), the reduction of the rms is from 15% (±3%) and up to 17% (±4%) along the G2 tracks. In the same way, considering T/P as the second satellite (Exp2b), a global reduction of near 12% (±3%) is obtained [13% (±4%) along G2 tracks].

In a statistical reconstruction study, Chelton and Schlax (2003) showed that SLA mapping capabilities are improved when combining J1 and T/P rather than J1 and EN. However, our results obtained by assimilating SLA observations with a high-resolution numerical model differ from those obtained by the simpler statistical algorithms. For a high-resolution model, it seems more beneficial to assimilate high across-track spatial resolution data (like EN data) in addition to J1, rather than additional high temporal resolution data (like T/P). This result is confirmed by Exp3 and Exp4. In addition, we see that the impact from the addition of G2 is higher than that from the addition of T/P (especially along J1 and EN tracks), even if G2 is used as a fourth satellite. Moreover, the limit of the spatial coverage of T/P and J1 is underlined by the neutral result obtained with Exp3 when looking at the signal along the J1 tracks; instead of reducing the rms of AMO, the assimilation of T/P data rather seems to induce a small increase of the error. This is certainly because T/P tracks are exactly between the J1 tracks. As a consequence, considering the 10-km Rossby radius of deformation in the Mediterranean Sea, the correction given by T/P is not propagated, or hardly so, on J1 tracks.

In most cases the representation of the mesoscales is optimal when four altimeters are used. The spatial distribution of the reduction of the mean rms of AMO (over the studied period) from one experiment to another is given in Fig. 6. The energetic areas [i.e., Ierapetra area, central Ionian and Algerian basin, as evidenced by Pujol and Larnicol (2005)] are clearly impacted from Exp0 to Exp1. The reduction of the rms of AMO reaches up to 30% in these areas. However, while a decrease of rms is observed in most of the points (global mean reduction of 13% of the rms), in some points it is increasing (up to 20%). The increase of errors when going from Exp0 to Exp1 is probably due to the nonuniform sampling scheme of J1 by itself, while in the case of two and three satellites the problem is alleviated, even if consistency between the raw signals of the satellites becomes an issue. In our case we use intercalibrated along-track products, which should have the most compatible signals between satellites. In any case, our work concentrates on the basin and time mean average values of the errors resulting from the addition of different satellites, and specific work on sub-areas should be done in the future.

The second satellite reduces the rms the most at points where there is the largest increase in rms caused by the first satellite. This indicates that the second satellite is complementary to the first, especially at the between-track location of the first satellite. The impact of the insertion of a second to a fourth altimeter is to refine the position, shape, and intensity of various eddies, especially in the areas of important mesoscale variability (e.g., the Algerian basin, Ionian basin, and Levantine Sea). Note that in terms of the reduction of the rms of the AMO, the impact of the second satellite (Exp2a and/or Exp2b) is almost as important as the contribution of the first satellite (Exp1). In fact, the mean rms reduction over the Mediterranean Sea is nearly 12% for EN (Exp2a) and nearly 10% for T/P (Exp2b). It locally reaches nearly 30% (in the Levantine Sea). The impact of the third and fourth satellites in term of rms reduction is lower: a reduction of around 3% is observed in Exp3 and Exp4. However, using a third and fourth satellite largely contributes to the precision of the analysis improving representation of position, intensity, and shape of predicted eddies.

The impact of the SLA assimilation can be also estimated by the surface eddy kinetic energy (EKE) of the analyses, as shown in Table 6. The assimilation of the first satellite (Exp1) induced an increase of the mean EKE of 27% with respect to the run with no assimilation (Exp0). However, the impact in terms of EKE of the assimilation of a second, third, or fourth satellite is different. Assimilation of EN (Exp2a) or T/P (Exp2b) as second satellites, respectively, leads to a 5% and 6% decrease of the EKE with respect to the one-satellite assimilated run (Exp1). With a third satellite assimilated (Exp3), an additional decrease of nearly 2% is registered. Finally, adding a fourth satellite (Exp4) leads to a 2% increase of the mean EKE with respect to Exp3. The mean EKE level for January 2005 captured by the model corrected with four satellites is nearly 200 cm^2 s^{-2}.

This behavior is quite different from that reported by Pascual et al. (2007) from altimetry reconstructed SLA with one and four satellites. The mapped products showed
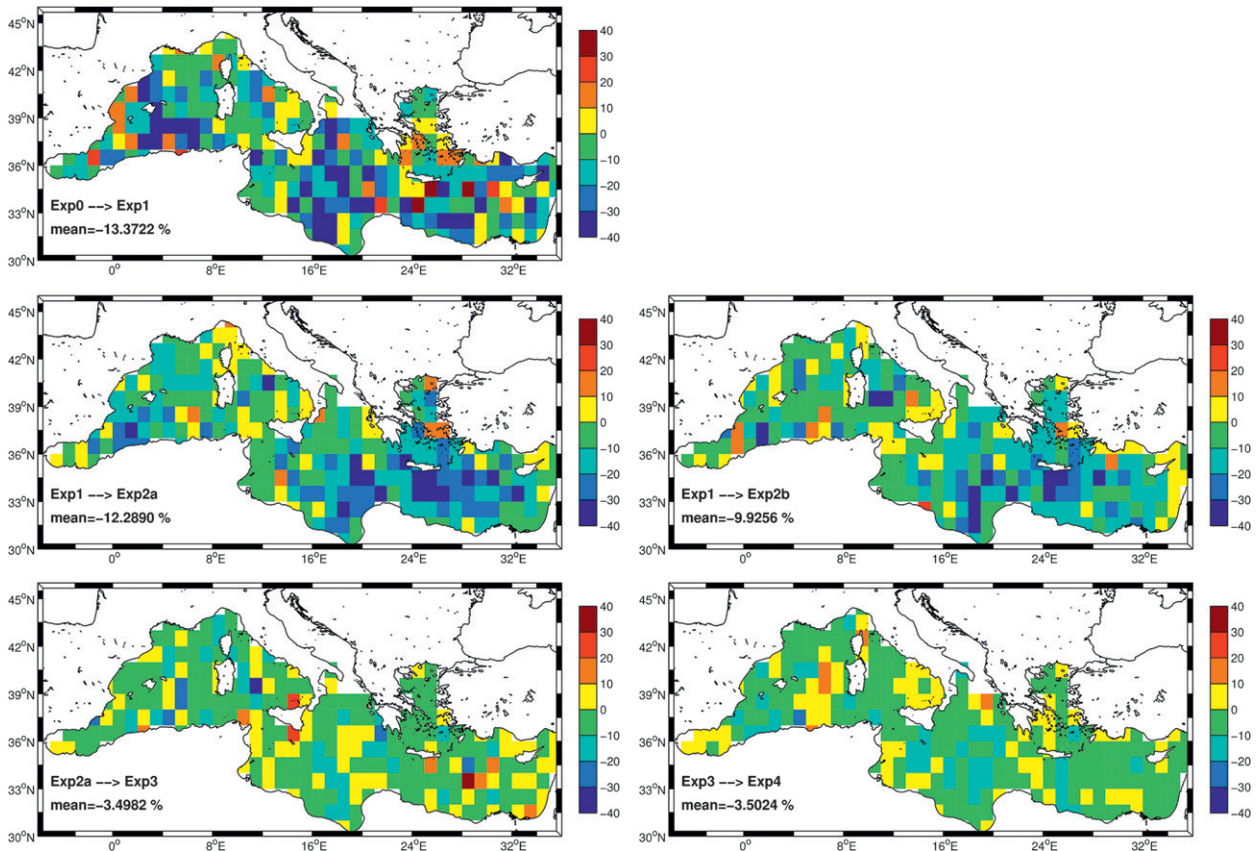
FIG. 6. Spatial distribution of the relative reduction of (top to bottom) AMO rms for SLA. Reduction of the rms is evidenced by negative values (green to blue).

a regular increase of the EKE from one to four satellites, that is, +40%, +10%, and +5% when two, three, and four satellites are merged. These differences make it evident that when assimilating SLA data in a high-resolution model, the introduction of mesoscale eddies does not automatically impact EKE because the corrections have to be dynamically adjusted by the model. Given a model horizontal and vertical resolution, the insertion of new structures in the sea level could modify only available potential energy, and some others will be dissipated by the model representation of viscosity and diffusion. The impact on EKE of sea level assimilation is connected to the dynamical adjustment by the model of the corrections, while in statistical reconstructions the addition of observations in areas of data voids automatically increases the kinetic energy of the flow field, but the result is probably dynamically unbalanced.

We now show the impact of altimetric data assimilation in the representation of specific structures of the circulation. This is the case, for example, of the Ierapetra Eddy (IE, which is usually located off the southeastern corner of Crete, Greece (Horton et al. 1994). This important structure of the circulation is known to be very

energetic and presents an important annual and interannual variability. It can detach from its usual position to migrate into the central Levantine Basin (Larnicol et al. 2002; Hamad et al. 2005). Without assimilation (Exp0) the IE is misplaced and weak, if not absent, in the model simulation (Fig. 7). Actually, IE formation processes are quite complex because they involve at least wind forcing (Horton et al. 1994) and water flow through the straits of the eastern Cretan Arc (Horton et al. 1997), while other forcings have also been claimed, such as bottom topography and water circulation in the Nord-Western Levantine Basin (Alhammoud 2005). Another difficulty of the accurate representation of IE comes from the importance of nonlinear terms in the dynamics of the eddy (Lermusiaux 2002). On the contrary, the

TABLE 6. Changes in the mean surface EKE over the Mediterranean Sea during January 2005, expressed in percent of the signal.

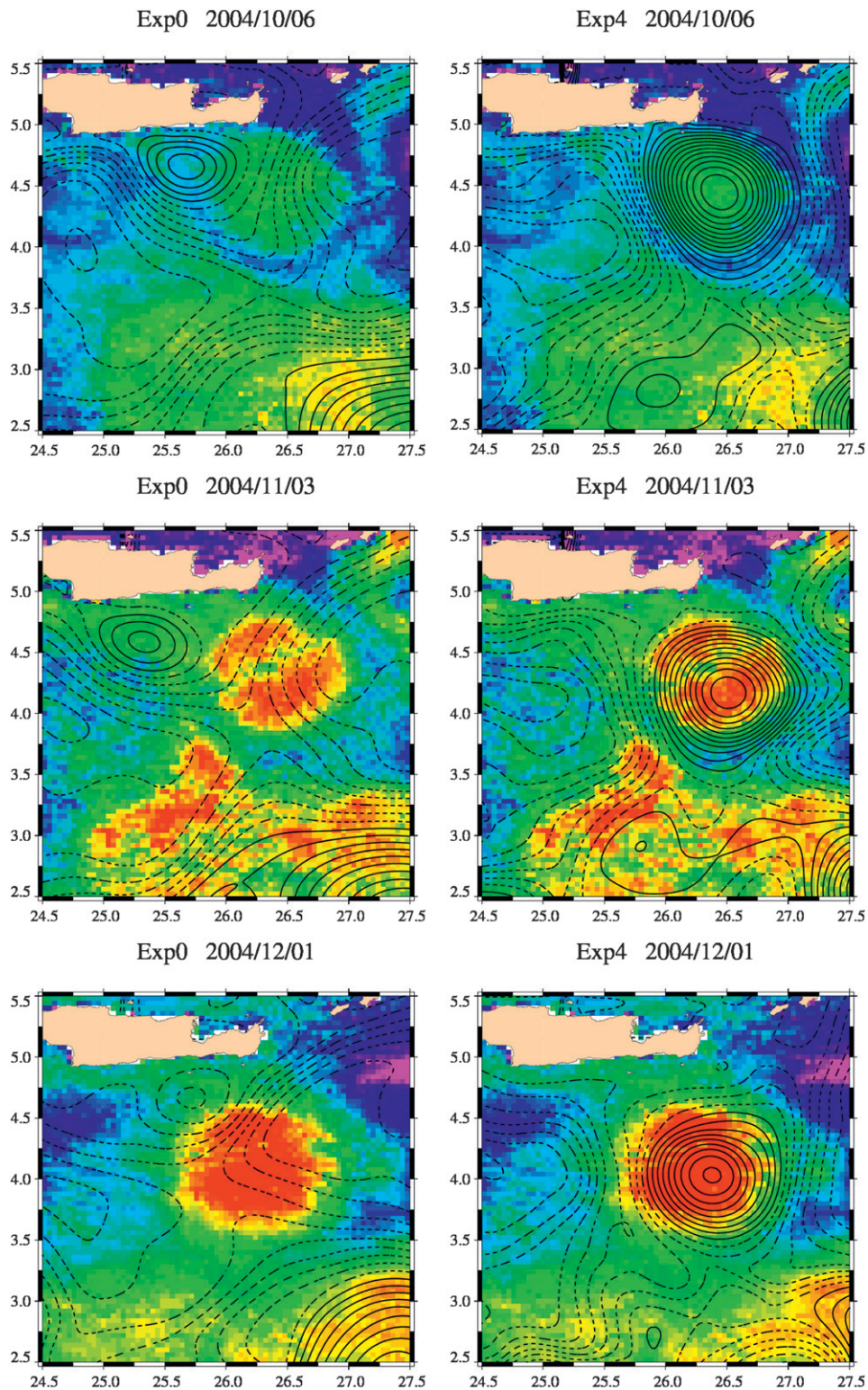| Exp0 → Exp1	Exp1 → Exp2a	Exp1 → Exp2b	Exp2a → Exp3	Exp3 → Exp4
+27	−5	−6	−2	+2

FIG. 7. SST maps over the IE area for (top to bottom) different days (experiments). Model SSH is superimposed with black isolines. The isolines range from −25 to 25 cm, with a 2-cm contour interval. Negative SSH (dashed lines) and positive SSH (solid lines); (left) simulation and (right) assimilation with four satellites; and warm waters (red) and cold waters (purple) are shown.
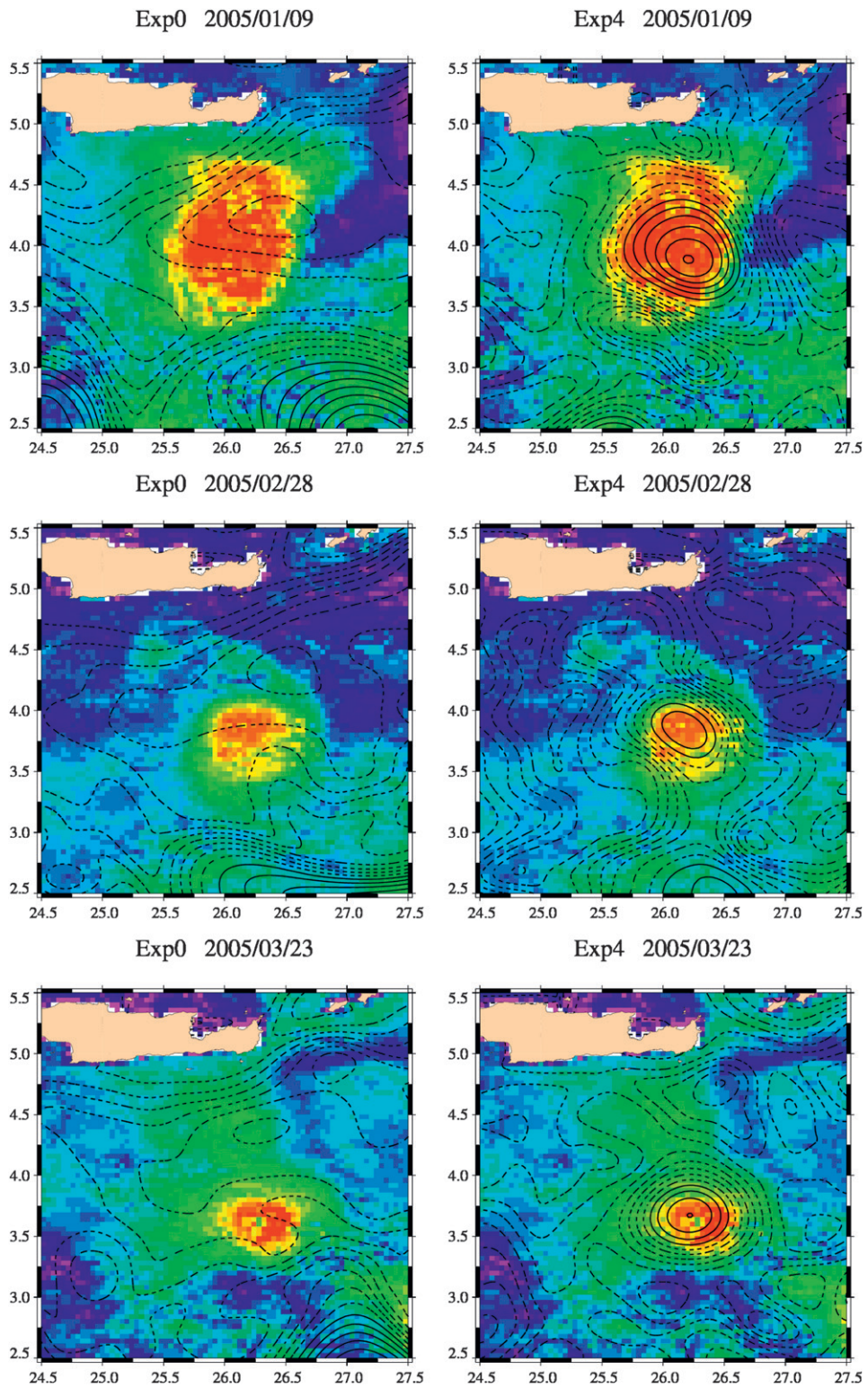
Exp0   2005/01/09

Exp4   2005/01/09

Exp0   2005/02/28

Exp4   2005/02/28

Exp0   2005/03/23

Exp4   2005/03/23

FIG. 7. (*Continued*)

assimilation of altimeter data introduced the IE in the analysis estimate. The position of the IE for different days is given in Fig. 7 superimposed to SST data. At the beginning of the studied period, IE was present in the simulation pressed against the southeastern corner of Crete (see the snapshot for 10 June 2004). Then, it detached from this position and slowly migrated southward. At the beginning of December 2004 it was centered around 34°N, 26.25°E, and it was visible around 33.5°N, 26.25°E at the end of March 2005. This behavior is similar to what has been known from the literature. The model analyses reproduce this behavior while the model simulation is seldom capable of resolving it.

Another improvement in the representation of eddies is shown for two anticyclonic eddies of the Algerian current. In Fig. 8 we show chlorophyll satellite data overlaid on the sea level analyses: one eddy is located around 36.9°N, 2.45°E and the second is at 37.1°N, 3.4°W. Without assimilation, the model simulation has a weak anticyclonic flow field detached from the coasts that does not correspond to the position and shape of the maxima in chlorophyll. As expected, the analysis improves with respect to the simulation if *J1* (Exp1) and then *EN* (Exp2a) are assimilated since the position of the anticyclonic structures seems to match better the chlorophyll observations. Contrary to what is observed with *EN*, the use of T/P as second satellite (Exp2b) seems to degrade the model output because the intensity of the western eddy is decreased and the eastern nearly disappears. On the contrary, combining T/P with *J1* and *EN* (Exp3) improves the representation of both eddies. Finally, the optimum analysis is obtained by assimilating the fourth altimeter *G2* (Exp4) and a nearly perfect correspondence of the two eddies is observed between the analyzed anticyclones and chlorophyll observations.

b. Impact of the number of altimeters on temperature and salinity analyses

To analyze the impact of multimission SLA assimilation on the temperature and salinity analysis fields, we compared the analyses of Exp0-Exp4 with Argo profiles as discussed in section 2c.

Results are reported in Table 4 for the different experiments. As mentioned before (section 3), assimilation of SLA only (Exp4) has a negative impact on AMO temperature bias and rms errors with respect to Exp0. For salinity, the assimilation of SLA with respect to the simulation has always had a positive impact. As shown in Table 4, smaller errors for salinity are obtained when the four satellites are assimilated and the error is decreased by the addition of each satellite.

The contribution of each satellite to the temperature reconstruction is more difficult to interpret: the specific combination of satellites seems to have different and contrasting impacts on the temperature reconstruction errors. A positive impact is observed when T/P is used as a second altimeter for both bias and rms, but a larger decrease in rms is obtained with the addition of *EN* as a second satellite. However, when both *EN* and T/P are added to *J1* (Exp3) the impact is small, or even negative, with respect to the single satellite case (Exp2a). If *G2* is used as a fourth satellite, the rms of AMO for temperature decreases, showing that even *G2* has a positive impact on the quality of the temperature analyses.

In terms of the impact of the different satellites on the quality of temperature and salinity reconstruction, our analysis is far from being conclusive. However, if XBT and Argo observations are combined to whatever combination of satellite SLA observations, the bias and rms errors in temperature and salinity profiles are always decreased (not shown). In section 2b we also point out that the absolute value of the bias and rms errors are now close to the observational error limits for the satellite SLA, and this limits our capability to understand small changes resulting from the addition of single satellites.

5. Summary and conclusions

This study has shown the impact of SLA assimilation on the quality of the analyses produced by an operational assimilation scheme in the Mediterranean Sea. A background error covariance matrix with a high spatial resolution was especially developed for this study, giving an improvement in the analysis reconstruction when all data—SLA and temperature and salinity profiles—are assimilated. Experiments were performed with five different altimeter combinations involving one to four satellites.

The experiments highlight the importance of multisatellite data assimilation in terms of quality of the analyses, measured as bias and rms of the differences between the analyses and the observations (AMO). In comparison with the model simulations (Exp0), the assimilation of SLA observations by one altimeter reduces the mean rms of AMO by more than 13%. The impact of the assimilation of a second satellite is nearly as important as that for the first satellite with more than 12% reduction of the mean rms of AMO. The impact of a second satellite especially underlines the complementarity with the first satellite, when a major rms reduction is locally observed in points where the first satellite assimilation introduced an rms increase. Impacts of a third and fourth altimeter are lower, but reductions of the AMO rms for SLA of 3% by each satellite are indicated. In some energetic areas, such as the Algerian current system, the assimilation
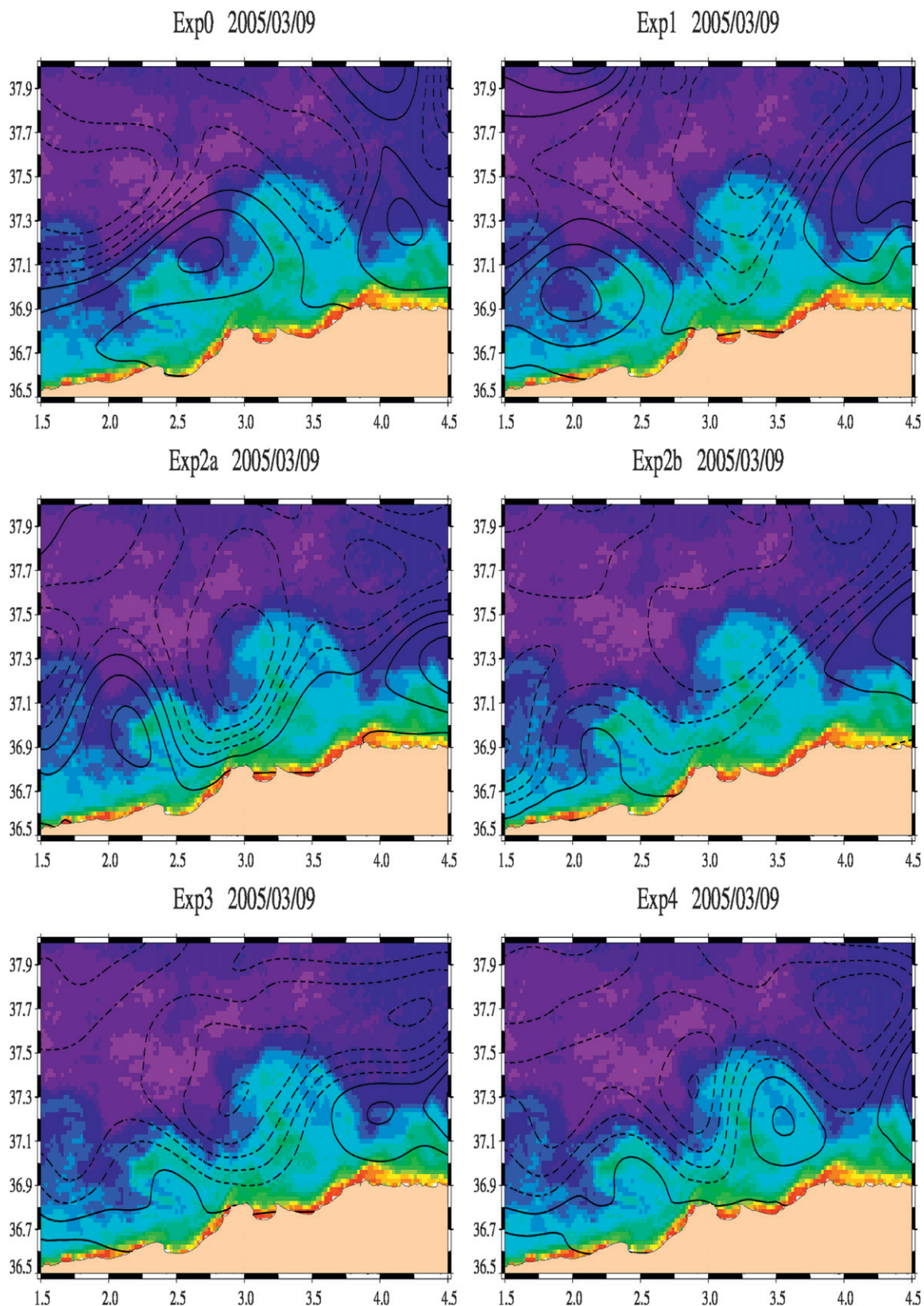
FIG. 8. Maps of chlorophyll along the Algerian Current observed during 9 Mar 2005. Model SSH is superimposed with black isolines from the six different experiments. The isolines range from −25 to 25 cm, with a 2-cm contour interval. Negative SSH (dashed lines) and positive SSH (solid lines) are shown. High concentrations of chlorophyll are presented (red), as are low concentrations (purple).

of observations from the fourth satellite reduced the rms of AMO by more than 10%.

The results obtained differentiate between spatial and temporal satellite sampling schemes. It is shown that high spatial resolution combined altimeters have a greater impact on the analyses. Although there is a certain probability that there is not a significant difference between Exp2a and Exp2b, it is more probable that *EN* as second satellite in addition to *J1* improves the analyses somewhat better than when T/P is added to *J1*. Moreover, the impact of *G2* as a fourth satellite is also important, or even a little bit more significant, than T/P as third satellite. The impact of *EN* is probably due to the high spatial resolution of the model, which allows the resolution of mesoscales that are better corrected by the high across-track resolution of *EN*. This result could support the concept of multimission altimetric monitoring done by complementary horizontal resolution satellites.

Comparison with independent temperature and salinity profiles confirms that the assimilation of more satellites improves the quality of the analyses, especially for salinity. The result is more questionable for temperature, an issue that will be treated in the future.

The EKE significantly increases by the assimilation of one altimeter. However, contrary to what was observed from altimeter-reconstructed fields without data assimilation (Pascual et al. 2007), once specific structures are introduced into the model with the assimilation of the first satellite, assimilation of additional altimeter data does not lead to a significant increase of the mean EKE. This might be associated with the specific model resolution, which allows a different dynamical adjustment of the assimilation corrections.

Our study shows that the inclusion of each of four altimeters has a significant impact on the accuracy of the analyses. We argue that the impact of the number of satellites on the data assimilation scheme depends on the data assimilation scheme approximations and the model capability to absorb the information from the observations. In the future the oceanographic models will have even higher horizontal resolutions. Therefore, we may expect that in the future the impact of additional altimeters should be reevaluated and assessed in light of the different model and analysis schemes.

APPENDIX

OceanVar Data Assimilation Scheme

The OceanVar scheme (Dobricic and Pinardi 2008) minimizes the following cost function:

$$J = \frac{1}{2}\delta\mathbf{x}^{\mathrm{T}}\mathbf{B}^{-1}\delta\mathbf{x} + \frac{1}{2}(\mathbf{d} - \mathbf{H}\delta\mathbf{x})^{\mathrm{T}}\mathbf{R}^{-1}(\mathbf{d} - \mathbf{H}\delta\mathbf{x}), \quad \text{(A1)}$$

where $\delta\mathbf{x}$ is the vector of analysis increments, $\mathbf{B}$ is the matrix of background error covariances, $\mathbf{d} = \mathbf{y} - H(\mathbf{x}_b)$ is the vector of misfits, $\mathbf{R}$ is the matrix of observational error covariances, $\mathbf{H}$ is the tangent linear approximation of the nonlinear observational operator H, $\mathbf{y}$ is the vector of observations, and $\mathbf{x}_b$ is the vector of the background state. Assuming that background and observational errors are independent, and that their corresponding error covariances are Gaussian, at the minimum of cost function (A1) the analysis state $\mathbf{x}_a = \mathbf{x}_b + \delta\mathbf{x}$ is the most probable for the given background state $\mathbf{x}_b$, observations $\mathbf{y}$, and the corresponding error covariances $\mathbf{B}$ and $\mathbf{R}$. To avoid the inversion of the matrix $\mathbf{B}$, a control variable $\mathbf{v}$ is defined by

$$\delta\mathbf{x} = \mathbf{V}\mathbf{v}, \quad \text{(A2)}$$

where $\mathbf{B} = \mathbf{V}\mathbf{V}^{\mathrm{T}}$. In the control space $\mathbf{v}$ the cost function becomes

$$J = \frac{1}{2}\mathbf{v}^{\mathrm{T}}\mathbf{v} + \frac{1}{2}(\mathbf{d} - \mathbf{H}\mathbf{V}\mathbf{v})^{\mathrm{T}}\mathbf{R}^{-1}(\mathbf{d} - \mathbf{H}\mathbf{V}\mathbf{v}). \quad \text{(A3)}$$

Furthermore, matrix $\mathbf{V}$ is modeled by the sequential application of linear operators $\mathbf{V} = \mathbf{V}_D\mathbf{V}_{u,v}\mathbf{V}_\eta\mathbf{V}_H\mathbf{V}_V$. Operator $\mathbf{V}_V$ consists of vertical EOFs with temperature and salinity error covariances. Therefore, control spaces $\mathbf{v}$ are weights that multiply the vertical EOFs, and $\mathbf{V}_V$ transforms them into vertical profiles of temperature and salinity increments. Vertical EOFs are eigenvectors with the largest eigenvalues estimated from the variability of a long-term model simulation around its mean value. The vertical profiles of temperature and salinity are further multiplied by the operator $\mathbf{V}_H$. It models horizontal Gaussian covariances depending on the horizontal distance in the presence of the coastlines. Operator $\mathbf{V}_\eta$ estimates the sea level and barotropic velocity increments for the given three-dimensional structure of temperature and salinity increments. It consists of a two-dimensional barotropic model forced by the vertically

integrated buoyancy force resulting from temperature and salinity increments. The model accurately finds the sea level increments even in areas with the highly variable and shallow bottom topography. Baroclinic components of velocity are estimated from the geostrophic relationship in the operator $\mathbf{V}_{u,v}$. At coastlines the geostrophic relationship is often incorrect and may produce the nondivergent velocity increments. The divergence along the coastlines is attenuated by operator $\mathbf{V}_D$, which applies the divergence damping filter. By sequentially applying different linear operators, the weights that multiply vertical covariances of temperature and salinity are transformed into a two-dimensional field of sea level increments and three-dimensional fields of temperature, salinity, and velocity increments by taking into account the coastlines and the bottom topography. The conversion from the control to the full physical space is performed in each iteration of the minimization in order to calculate cost function (A3). In addition, it is necessary in each iteration to calculate the gradient of the cost function by applying the adjoint of the observational and transformation linear operators that substitute transpose of matrices in

$$\nabla J = \mathbf{v} + \mathbf{V}^T \mathbf{H}^T \mathbf{R}^{-1} (\mathbf{d} - \mathbf{H}\mathbf{V}\mathbf{v}). \qquad \text{(A4)}$$

Once the minimum is found in the control space, the model correction is calculated by applying Eq. (A2). OceanVar is a three-dimensional variational scheme, because it applies estimates of vertical temperature and salinity error covariances that are independent of actual model dynamics.

REFERENCES

Alhammoud, B., 2005: Oceanic general circulation and mesoscale variability in the eastern Mediterranean Sea: Numerical approach. Ph.D. thesis, Université de la Mediterranée Aix Marseille II, 210 pp.

AVISO, 2009: Ssalto/Duacs user handbook: (M)SLA and (M)ADT near-real time and delayed time products. Edition 1.10, SALP-MU-P-EA-21065-CLS, 52 pp. [Available online at http://www.aviso.oceanobs.com/fileadmin/documents/data/tools/hdbk_duacs.pdf.]

Benkiran, M., 2007: Altimeter data assimilation in the Mercator Ocean System. *Mercator Ocean Quarterly Newsletter,* Vol. 25, April 2007, Mercator Ocean, 32–39. [Available online at http://www.mercator-ocean.fr/documents/lettre/lettre_25_en.pdf.]

Berry, P. J., and J. C. Marshall, 1989: Ocean modelling studies in support of altimetry. *Dyn. Atmos. Oceans,* **13,** 269–300.

Buongiorno Nardelli, B., G. Larnicol, E. D'Acunzo, R. Santoleri, S. Marullo, and P. Y. Le Traon, 2003: Near real time SLA and SST products during 2 years of MFS pilot project: Processing, analysis of the variability and of the coupled patterns. *Ann. Geophys.,* **21,** 103–121.

Carrère, L., and F. Lyard, 2003: Modeling the barotropic response of the global ocean to barotropic wind and pressure forcing—Comparisons with observations. *Geophys. Res. Lett.,* **30,** 1275, doi:10.1029/2002GL016473.

Chelton, D., and M. Schlax, 2003: The accuracies of smoothed sea surface height field constructed from tandem satellite altimeter datasets. *J. Atmos. Oceanic Technol.,* **20,** 1276–1302.

De Mey, P., and A. R. Robinson, 1987: Assimilation of altimeter eddy fields in a limited-area quasi-geostrophic model. *J. Phys. Oceanogr.,* **17,** 2280–2293.

Demirov, E., N. Pinardi, C. Fratianni, M. Tonani, L. Giacomelli, and P. De Mey, 2003: Assimilation scheme of the Mediterranean Forecasting System: Operational implementation. *Ann. Geophys.,* **21,** 189–194.

Dobricic, S., 2005: New mean dynamic topography of the Mediterranean calculated from assimilation system diagnostics. *Geophys. Res. Lett.,* **32,** L11606, doi:10.1029/2005GL022518.

——, and N. Pinardi, 2008: An oceanographic three-dimensional variational data assimilation scheme. *Ocean Modell.,* **22,** 89–105.

——, ——, M. Adani, A. Bonazzi, C. Fratianni, and M. Tonani, 2005: Mediterranean Forecasting System: An improved assimilation scheme for sea-level anomaly and its validation. *Quart. J. Roy. Meteor. Soc.,* **131,** 3627–3642, doi:10.1256/qj.05.100.

——, ——, ——, M. Tonani, C. Fratianni, A. Bonazzi, and V. Fernandez, 2007: Daily oceanographic analyses by Mediterranean Forecasting System at the basin scale. *Ocean Sci.,* **3,** 149–157.

Ducet, N., P.-Y. Le Traon, and G. Reverdin, 2000: Global high-resolution mapping of ocean circulation from TOPEX/Poseidon and ERS-1 and -2. *J. Geophys. Res.,* **105,** 19 477–19 498.

Ezer, T., and G. L. Mellor, 1994: Continuous assimilation of Geosat altimeter data into a three-dimensional primitive equation Gulf Stream model. *J. Phys. Oceanogr.,* **24,** 832–847.

Fukumori, I., R. Raughunath, L. Fu, and Y. Chao, 1999: Assimilation of TOPEX/Poseidon altimeter data into a global ocean circulation model: How good are the results? *J. Geophys. Res.,* **104,** 25 647–25 665.

——, D. Menemenlis, and T. Lee, 2006: A near-uniform basin-wide sea level fluctuation of the Mediterranean Sea. *J. Phys. Oceanogr.,* **37,** 338–358.

Haines, K., 2002: Assimilation of satellite altimetry in ocean models. *Ocean Forecasting: Conceptual Basis and Applications,* N. Pinardi and J. D. Woods, Eds., Springer, 117–130.

Hamad, N., C. Millot, and I. Taupier-Letage, 2005: The surface circulation in the eastern basin of the Mediterranean Sea. *Sci. Mar.,* **70,** 457–503.

Holland, W. R., and P. Malanotte-Rizzoli, 1989: Assimilation of altimeter data into an ocean circulation model: Space versus time resolution studies. *J. Phys. Oceanogr.,* **19,** 1507–1534.

Horton, C., J. Kerling, G. Athey, J. Schmitz, and M. Clifford, 1994: Airborne expendable bathythermograph surveys of the eastern Mediterranean. *J. Geophys. Res.,* **99,** 9891–9905.

——, M. Clifford, J. Schmitz, and L. H. Kantha, 1997: A real-time oceanographic nowcast/forecast system for the Mediterranean Sea. *J. Geophys. Res.,* **102** (C11), 25 123–25 156.

Ivchenko, V. O., S. D. Danilov, D. V. Sidorenko, J. Schröter, M. Wenzel, and D. L. Aleynik, 2007: Comparing the steric height in the Northern Atlantic with satellite altimetry. *Ocean Sci.,* **3,** 485–490.

Larnicol, G., N. Ayoub, and P.-Y. Le Traon, 2002: Major changes in the Mediterranean Sea level variability from 7 years of TOPEX/Poseidon and ERS-1/2 data. *J. Mar. Syst.,* **33–34,** 63–89.

Lermusiaux, P. F. J., 2002: On the mapping of multivariate geophysical fields: Sensitivities to size, scales, and dynamics. *J. Atmos. Oceanic Technol.,* **19,** 1602–1637.

——, P. Malanotte-Rizzoli, D. Stammer, J. Carton, J. Cummings, and A. M. Moore, 2006: Progress and prospects of U.S. data assimilation in ocean research? *Oceanography,* **19,** 172–183.

Le Traon, P.-Y., 2002: Satellite oceanography for ocean forecasting. *Ocean Forecasting: Conceptual Basis and Applications,* N. Pinardi and J. D. Woods, Eds., Springer, 19–36.

——, and P. Gauzelin, 1997: Response of the Mediterranean mean sea level to atmospheric pressure forcing. *J. Geophys. Res.,* **102,** 973–984.

——, and F. Ogor, 1998: ERS-1/2 orbit improvement using TOPEX/POSEIDON: The 2-cm challenge. *J. Geophys. Res.,* **103,** 8045–8057.

Madec, G., P. Delecluse, M. Imbard, and C. Levy, 1998: OPA 8.1 general circulation model reference manual. Note du Pole de modélisation, Institut Pierre-Simon Laplace, Université Pierre et Marie Curie Tech. Note 11, 97 pp. [Available online at http://www.nemo-ocean.eu/content/download/259/1665/version/1/file/Doc_OPA8.1.pdf.]

Masina, S., N. Pinardi, and A. Navarra, 2001: A global ocean temperature and altimeter data assimilation system for studies of climate variability. *Climate Dyn.,* **17,** 687–700.

Mellor, G. L., and T. Ezer, 1991: A Gulf Stream model and an altimetry assimilation scheme. *J. Geophys. Res.,* **96,** 8779–8795.

——, and ——, 1995: Sea level variations induced by heating and cooling: An evaluation of the Boussinesq approximation in ocean models. *J. Geophys. Res.,* **100** (C10), 20 565–20 577.

Ménard, Y., and Coauthors, 2003: The Jason-1 mission. *Mar. Geod.,* **26,** 131–146.

Millot, C., 1999: Circulation in the western Mediterranean Sea. *J. Mar. Syst.,* **20,** 423–442.

——, and I. Taupier-Letage, 2005: Circulation in the Mediterranean Sea. *The Mediterranean Sea,* A. Sailot, Ed., Vol. 5K, *The Handbook of Environmental Chemistry,* Springer, 29–66.

Oddo, P., M. Adani, N. Pinardi, C. Fratianni, M. Tonani, and D. Pettenuzzo, 2009: A nested Atlantic-Mediterranean Sea general circulation model for operational forecasting. *Ocean Sci.,* **5,** 461–473.

Oey, L.-Y., T. Ezer, G. Forristall, C. Cooper, S. DiMarco, and S. Fan, 2005: An exercise in forecasting loop current and eddy frontal positions in the Gulf of Mexico. *Geophys. Res. Lett.,* **32,** L12611, doi:10.1029/2005GL023253.

Pascual, A., M.-I. Pujol, G. Larnicol, P.-Y. Le Traon, and M.-H. Rio, 2007: Mesoscale mapping capabilities of multisatellite altimeter missions: First results with real data in the Mediterranean Sea. *J. Mar. Syst.,* **65,** 190–211.

Pinardi, N., and G. Coppini, 2010: Operational oceanography in the Mediterranean Sea: The second stage of development. *Ocean Sci.,* **6,** 263–267.

——, and Coauthors, 2003: The Mediterranean ocean forecasting system: First phase of implementation (1998–2001). *Ann. Geophys.,* **21,** 3–20.

Pujol, M.-I., and G. Larnicol, 2005: Mediterranean Sea eddy kinetic energy variability from 11 years of altimetric data. *J. Mar. Syst.,* **58,** 121–142.

Poulain, P.-M., and Coauthors, 2007: MedArgo: A drifting profiler program in the Mediterranean Sea. *Ocean Sci.,* **3,** 379–395.

Rio, M.-H., P.-M. Poulain, A. Pascual, E. Mauri, G. Larnicol, and R. Santoleri, 2007: A mean dynamic topography of the Mediterranean Sea computed from altimetric data, in-situ measurements and a general circulation model. *J. Mar. Syst.,* **65,** 484–508.

Robinson, A. R., and P. F. J. Lermusiaux, 2001: Data assimilation in models. *Encyclopedia of Ocean Sciences,* S. A. Thorpe and K. K. Turekian, Eds., Academic Press, 623–634.

——, W. G. Leslie, A. Theocharis, and A. Lascaratos, 2001: Mediterranean Sea circulation. *Encyclopedia of Ocean Sciences,* S. A. Thorpe and K. K. Turekian, Eds., Academic Press, 1689–1706.

Tonani, M., N. Pinardi, S. Dobricic, I. Pujol, and C. Fratianni, 2008: A high-resolution free-surface model of the Mediterranean Sea. *Ocean Sci.,* **4,** 1–14.